sciendo

CrossMark

Moroccan J. of Pure and Appl. Anal. (MJPAA)
Volume 9(1), 2023, Pages 01–26
ISSN: Online 2351-8227 - Print 2605-6364
DOI: 10.2478/mjpaa-2023-0001

Numerical comparison of three a posteriori error estimators for nonconforming finite element method

B. Achchab[1], A. Agouzal[2], K. Bouihat[3], A. Majdoubi[4]

Abstract. In this paper, we propose to compare three a posteriori error estimators namely equilibrated, star-based and residual based for the Poisson problem and the Stokes problem with lowest-order Crouzeix-Raviart finite element discretization. The numerical results are presented to compare the performance of the three estimators in an adaptive refinement strategy.

Mathematics Subject Classification (2020). 35A35; 65N15; 65N30; 65N50 and 76M10.
Key words and phrases. Nonconforming finite elements; Adaptive finite element method; Comparison; A posteriori error estimates.

1. Introduction

The finite element method [27] is one of the most well-known methods used for the numerical approximation of partial differential equations, thanks to its theoretical richness and its

Received : November 26, 2022 - Accepted : December 28, 2022.

[1,3] *University Hassan 1st, LAMSAD, ENSA Berrechid B.P. 218 Berrechid 26100, Morocco*
e-mail[1]: boujemaa.achchab@uhp.ac.ma (Corresponding Author).,
e-mail[3]: khalid.bouihat@uhp.ac.ma

[2]*Department of Mathematics, U.M.R. 5208 - Camille Jordan Institute, Lyon 1 University. Building 1001,69 622 Villeurbanne Cedex - France*
e-mail[2]: abdellatif.agouzal@univ-lyon1.fr

[4]*Laboratory of Engineering Sciences, National School of Applied Sciences, Ibn Tofail University, Kenitra, Morocco*
e-mail[4]: adil.majdoubi@uit.ac.ma

.

wide field of applications. The non-conforming finite element methods [28] have received a lot of attention recently, Due to the simplicity and small support sets of basis functions of these elements. A posteriori error estimators are now essential tools for the accurate and effective computation of partial differential equations. These estimators allow to estimate explicitly the error of approximation and consequently ensure control of this error. A posteriori error analysis for nonconforming lowest-order Crouzeix-Raviart finite element methods can be found in [7, 31, 9, 32, 8, 6, 2, 23, 5, 4, 45, 44]. In the literature, there are different types of a posteriori error estimators to control the exact error. Then a natural question arises: what is the most suitable estimator? In this sense, some work these last years has been achieved, which compares estimators for some problems. In [13], Bank et al. compare certain estimates based on the resolution of local Stokes systems versus estimates based on the residuals of discretized finite element equations. Carstensen et al. in [25] present a unified a posteriori error analysis for a wide range of discontinuous Galerkin finite element methods, applied to the Laplace, Stokes, and Lamé equations. In [21] they compare some a posteriori error estimators for the Poisson problem with lowest-order finite element discretization. Residual-based error estimators compete with a wide range of averaging estimators and estimators based on local problems. In [22] they present a survey and a computational comparison in the lowest-order case, and in [26] they present a survey where they compare different strategies for guaranteed error control for the lowest-order nonconforming Crouzeix-Raviart finite element method for the Stokes equations. In this paper, we compare three a posteriori error estimators for Poisson problem and the Stokes problem with lowest-order Crouzeix-Raviart finite element discretization. The first is the Equilibration estimator [35, 31, 41, 1, 5, 10], the second is the star-based estimator [42, 4] and the third is the residual estimator [29, 30].
The remaining parts of this paper are outlined as follows, Section 2 introduces the setting for the Poisson model problem. The three error indicators that we want to compare are introduced and we conclude this section by presenting two numerical results. Section 3 deals with Stokes model problem, after introducing the setting and notations, we present the three estimators for this problem and compare them in two numerical examples.

2. Poisson problem

2.1. Problem setting, notations and discrete problem. Let Ω be a simply connected polygonal domain of $\mathbb{R}^d$, $d = 2$, with a lipschitzian boundary and $f \in L^2(\Omega)$. we consider the simple elliptic model problem : Find u such that

$$\begin{cases} -\Delta u &= f & \text{in } \Omega, \\ u &= 0 & \text{on } \partial\Omega. \end{cases} \tag{2.1}$$

Let $\mathcal{T}_h$ be a triangulation in the d-simplex of Ω that is regular and conforming in Ciarlet's sense [27, p. 38]. For every d-simplex $T \in \mathcal{T}_h$, we will denote by h_T the diameter of T, $meas_d(T)$ the measure of T in $\mathbb{R}^d$ and E_T the set of edges of T.

We consider V_h be the Crouzeix-Raviart finite element space defined by :

$$V_h = \{v \in L^2(\Omega) \,|\, \forall T \in \mathcal{T}_h, v|_T \in P_1(T), \forall E \in E_h^I, \int_E [v]_E \, ds = 0; \\ \forall E \in E_h^F, \int_E v \, ds = 0\}, \tag{2.2}$$

where E_h^I (resp. E_h^F) denotes the set of internal (resp. boundary) edges (faces) of $\mathcal{T}_h$ and $[\cdot]_E$ denotes the jump through E. In Figure 1, This finite element is represented in Figure 1 for d = 2 and d = 3; in three dimensions, just the visible degrees of freedom are shown.

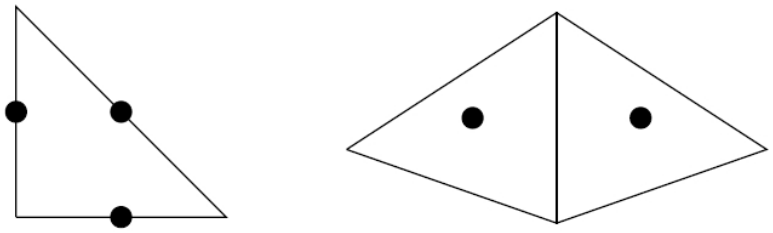

FIGURE 1. Crouzeix-Raviart finite element in two (left) and three (right) dimensions.

We choose an arbitrary normal direction n for an interior edge E, if $n = (n_1, n_2)^t$, we define the tangent $t = (-n_2, n_1)^t$. n is the outward normal when E is a boundary edge.
We denote by $\{x_i\}_{i\in\mathcal{N}}$ the set of all nodes of the triangulation $\mathcal{T}_h$, where $\mathcal{N}$ the cardinal number of this set. In the paper, by $i \in \mathcal{N}$ we will refer to the node x_i and ϕ_i denotes the canonical continuous piecewise linear basis function associated to x_i. The star ω_i is the interior relative to Ω of the support of ϕ_i, and h_i is the maximal size of the elements constituting ω_i. Finally, Γ_i denotes the union of the edges (faces) touching x_i that are contained in Ω, and $\overline{\Gamma}_i$ the union of the edges (faces) touching x_i that are contained in $\overline{\Omega}$. h_E denotes the size (diameter) of an edge (face) E.
For each star ω_i, $i \in \mathcal{N}$, we introduce the space $V(\omega_i)$ defined by

$$V(\omega_i) = \{v \in H^1_{loc}(\omega_i) \,|\, \int_{\omega_i} v\phi_i \, dx = 0\}, \qquad \text{if } x_i \text{ is an interior node,}$$

and

$$V(\omega_i) = \{v \in H^1_{loc}(\omega_i) \,|\, v = 0 \ \text{ on } \partial\omega_i \cap \Gamma\}, \qquad \text{if } x_i \text{ is a boundary node.}$$

The nonconforming finite element approximation of the problem (2.1) is as follows :

$$\begin{cases} \text{find } u_h^{NC} \in V_h \text{ such that} \\ \\ \displaystyle\sum_{T\in\mathcal{T}_h} \int_T \nabla u_h^{NC} \cdot \nabla v_h \, dx = \sum_{T\in\mathcal{T}_h} \int_T f v_h \, dx \quad \forall v_h \in V_h \cap H_0^1(\Omega). \end{cases} \tag{2.3}$$

We refer the reader to [28] for convergence analysis of the approximate solution.

2.2. Equilibration estimator. Thanks to the Prager-Synge equality [43] and the hypercircle method, these estimators came to light through Ladevèze [41]. The construction of a flux belonging to $H(div)$ represents the major difficulty of this approach. This construction is made by post-processing or the resolution of local problems. In the literature, this type of estimator has been presented, for conforming finite elements, by Luce-Wohlmuth [41] and Braess-Schoberl [18], one can also cite [34, 37, 50]. For nonconforming finite elements, we find [31], Achchab [1, 6, 5], Ainsworth [9], Kim [40] and Braess [17].

In this subsection, we present an a posteriori error estimator developed by Achchab et al. in [5] for the P_1-nonconforming finite element approximation. We adopt the error using a flux reconstruction approach.

Let $\widetilde{u}_h$ be an element of $H_0^1(\Omega)$, a conforming post-processing of u_h^{NC} computed by using the Oswald interpolation operator [19, 33, 38], and we consider the vector function $\mathbf{p}_h$ defined by

$$\forall T \in \mathcal{T}_h, \quad \mathbf{p}_{h|T} = \frac{1}{meas_d(T)} \int_T \nabla u_h^{NC} - \sum_{E \in E_T} \left(\int_T f \mu^E \, dx \right) \mathbf{p}_h{}^E, \tag{2.4}$$

where

$$\mu^E = 1 - d \times \lambda \quad \text{in } T, \tag{2.5}$$

here λ is the unique function of $P_1(T)$ vanishing on E and whose value is 1 on the vertex of T opposite to E and

$$\mathbf{p}_h{}^E{}_{|T} = \frac{\mathbf{x} - \mathbf{v_E}}{d \times meas_d(T)}, \tag{2.6}$$

where $\mathbf{v}_E$ is the vertex of T opposite to E. Note that $\mathbf{p}_h$ in an element of $H(div, \Omega)$ satisfying a local equilbrium equation.

Concerning the a posteriori error estimator for $u - u_h^{NC}$, we have

Theorem 2.1. *For $\widetilde{u}_h \in H^1(\Omega)$ and $\mathbf{p}_h$ definid in (2.4), we have*

$$\begin{aligned} \sum_{T \in \mathcal{T}_h} \|\nabla(u - u_h^{NC})\|_{0,T}^2 \leq 4 \| \mathbf{p}_h - \nabla \widetilde{u}_h\|_{0,\Omega}^2 + 2 \sum_{T \in \mathcal{T}_h} \|\nabla(u_h^{NC} - \widetilde{u}_h)\|_{0,T}^2 \\ 16 \sum_{T \in \mathcal{T}_h} \mu^2 h_T^2 \| \operatorname{div} \mathbf{p}_h + f\|_{0,T}^2, \end{aligned} \tag{2.7}$$

and For all $T \in \mathcal{T}_h$ we have

$$\| \mathbf{p}_h - \nabla \widetilde{u}_h\|_{0,T} \leq \| \mathbf{p}_h - \mathbf{p}\|_{0,T} + \|\nabla u - \nabla \widetilde{u}_h\|_{0,T}, \tag{2.8}$$

where

$$\mu = \inf_{0 \leq \varepsilon < 1/2} \frac{\left(\int_0^1 (1-t)^{2\varepsilon} \min(t^{-d}, (1-t)^{-d}) \, dt \right)^{1/2}}{(1-2\varepsilon)^{1/2}}. \tag{2.9}$$

For proof of theorem see [5].

2.3. Star-based estimators. Introduced by Babuška [11], and Bernardi [15], then analyzed and generalized by various authors including Bank [12, 13, 14], Verfürth [47, 48], and Hoppe [51]. These estimators are obtained by locally solving simpler problems than the initial problem. The right-hand sides of these equations are the residuals of the main equation, and the indicators are appropriate norms of these solutions. The global estimator is obtained by summing the norms of each local indicator. For more details see references [18, 20]. Nochetto et al [42] analyzed this type of estimator in the conforming finite elements case, based on solving local problems on stars; a star is the support of a piecewise linear nodal basis function. In this subsection, we introduce an a posteriori error estimator developed in [4, 16] for low-order nonconforming approximation of scalar second-order elliptic problem, based on the resolution of local problems on stars.

We define the finite dimensional local spaces $\mathcal{P}_0^2(\omega_i)$ as follows,

Definition 2.1. *For $i \in \mathcal{N}$, let $\mathcal{P}^2(\omega_i)$ represent the space of continuous piecewise quadratic functions on star ω_i that vanish on $\partial\omega_i$. The spaces $\mathcal{P}_0^2(\omega_i)$ is defined by $\mathcal{P}_0^2(\omega_i) = \mathcal{P}^2(\omega_i) \cap V(\omega_i)$.*

Let us introduce the usual H^1-norm on ω_i,

$$||u||^2_{1,\omega_i} = \|\nabla u\|^2_{0,\omega_i} + \|u\|^2_{0,\omega_i}.$$

For each $i \in \mathcal{N}$, we take into account the local problems :

$$(P_i) \quad \begin{cases} \text{Find } \eta_i \in \mathcal{P}_0^2(\omega_i) \text{ such that } \forall \mu_i \in \mathcal{P}_0^2(\omega_i), \\ \displaystyle\int_{\omega_i} (\nabla\eta_i \cdot \nabla\mu_i)\phi_i\, dx = \int_{\omega_i} (\nabla u_h^{NC} \cdot \nabla\mu_i)\phi_i\, dx - \int_{\omega_i} f\mu_i\phi_i\, dx. \end{cases}$$

Using Lax-Milgram Theorem, we can prove that each discrete problem (P_i) admits a unique solution η_i. Now we introduce the local error indicators,

$$\forall i \in \mathcal{N}, \forall u_h^{NC} \in V_h, \quad E^2_{1,i}(u_h^{NC}) = \int_{\omega_i} |\nabla\eta_i|^2\phi_i\, dx, \tag{2.10}$$

$$\forall i \in \mathcal{N}, \forall u_h^{NC} \in V_h, \quad E^2_{2,i}(u_h^{NC}) = \sum_{E\in\omega_i} h^{-1}||[u_h^{NC}]_E||_{0,E} \tag{2.11}$$

and set the problem data oscillation,

$$osc(f) = \Big(\sum_{i\in\mathcal{N}} h_i^2 \|(f - f_i)\phi_i^{\frac{1}{2}}\|^2_{0,\omega_i}\Big)^{\frac{1}{2}}. \tag{2.12}$$

where $f_i = \dfrac{\int_{\omega_i} f\phi_i\, dx}{\int_{\omega_i} \phi_i\, dx}$ for interior nodes, and $f_i = 0$ otherwise.

The following theorem gives the upper bound of the error.

Theorem 2.2. *Let $u_h^{NC} \in V_h$ be a solution of (2.3). We have*

$$\Big(\sum_{i\in\mathcal{N}} \|u - u_h^{NC}\|^2_{1,\omega_i}\Big)^{\frac{1}{2}} \le C_1 \left[\Big(\sum_{i\in\mathcal{N}} E^2_{1,i}(u_h^{NC})\Big)^{\frac{1}{2}} + \Big(\sum_{i\in\mathcal{N}} E^2_{2,i}(u_h^{NC})\Big)^{\frac{1}{2}} + osc(f)\right], \tag{2.13}$$

where C_1 depends only on the minimum angle of $\mathcal{T}_h$.

The following theorem provides the lower bound of the error without oscillation.

Theorem 2.3. *Let $u_h^{NC} \in V_h$, there exists a positive constant C_2 , depending on the minimum angle of the triangulation such that, for any $i \in \mathcal{N}$,*

$$E_{1,i}(u_h^{NC}) \leq C_2 ||u - u_h^{NC}||_{1,\omega_i}, \tag{2.14}$$

and

$$E_{2,i}(u_h^{NC}) \leq C_2 \left(\sum_{j \in \mathcal{N}} \|u - u_h^{NC}\|_{1,\omega_j}^2 \right)^{\frac{1}{2}}. \tag{2.15}$$

For proofs of two Theorems see [4].

2.4. Residual estimators. Initiated by Babuška and Rheinboldt [11] and detailed by Verfürth [48], are probably the most popular. These are explicit error estimators involving residuals from equilibrium equations and jumps from normal stresses to interfaces. They apply to elliptical problems (Poisson, Stokes, or linear elasticity) in dimension 2 or 3. Upper bounds are generally computable bounds multiplied by a constant independent of the exact solution and the step of the mesh but whose value is difficult to calculate explicitly; However, let us mention the works of Verfürth [49], Carstensen-Funken [24], and Veeser-Verfürth [46]. In this subsection, we present residual-based error estimator developed by Dari et al. in [29] for the P_1-nonconforming finite element approximation of the Poisson problem and a general reliability result.

For a side E define $J_{E,n}$ and $J_{E,t}$ by

$$J_{E,n} = \begin{cases} [\nabla u_h \cdot n]_E & \text{if} \quad E \in E_h^I \\ \\ 0 & \text{if} \quad E \in E_h^F \end{cases} \tag{2.16}$$

and

$$J_{E,t} = \begin{cases} [\nabla u_h \cdot t]_E & \text{if} \quad E \in E_h^I \\ \\ -2\nabla u_h \cdot t & \text{if} \quad E \in E_h^F \end{cases} \tag{2.17}$$

with this notation we introduce the local error estimator η_T defined by.

$$\eta_T^2 = meas_d(T)\|f\|_{0,T}^2 + \frac{1}{2} \sum_{E \in E_T} h_E^2 (|J_{E,n}|^2 + |J_{E,t}|^2), \tag{2.18}$$

and the global one is given by

$$\eta^2 = \sum_{T \in \mathcal{T}_h} \eta_T^2.$$

We have the following result :

Theorem 2.4. *There exist positive constants C_3 and C_4 depending only on the domain Ω and the minimum angle of $\mathcal{T}_h$ such that*

$$C_3\,\eta \leq \left(\sum_{T\in\mathcal{T}_h} \|\nabla(u-u_h^{NC})\|_{0,T}^2\right)^{1/2} \leq C_4\,\eta \tag{2.19}$$

For proof of theorem see [29].

2.5. Numerical experiments. In this subsection, we compare the estimators presented for the Poisson problem and that we will denote as follows

$$\eta_1 := \left(4\|\,\mathbf{p}_h - \nabla\widetilde{u}_h\|_{0,\Omega}^2 + 2\sum_{T\in\mathcal{T}_h}\|\nabla(u_h^{NC}-\widetilde{u}_h)\|_{0,T}^2 + 16\sum_{T\in\mathcal{T}_h}\mu^2h_T^2\|\operatorname{div}\,\mathbf{p}_h + f\|_{0,T}^2\right)^{\frac{1}{2}}, \tag{2.20}$$

$$\eta_2 := \Big(\sum_{i\in\mathcal{N}} E_{1,i}^2(u_h^{NC})\Big)^{\frac{1}{2}} + \Big(\sum_{i\in\mathcal{N}} E_{2,i}^2(u_h^{NC})\Big)^{\frac{1}{2}} + \ osc(f), \tag{2.21}$$

$$\eta_3 := \left(\sum_{T\in\mathcal{T}_h}(meas_d(T)\|f\|_{0,T}^2 + \frac{1}{2}\sum_{E\in E_T} h_E^2(|J_{E,n}|^2 + |J_{E,t}|^2))\right)^{\frac{1}{2}}. \tag{2.22}$$

They are tested with the following iterative algorithm:

Algorithm 1

1: Generate a starting mesh, then calculate the solution.
2: Calculate local error indicators and their sum.
3: Refine the mesh in the areas where the indicators are bigger than their mean value and compute solution.
4: **if** stopping criterium is satisfied, **then** STOP.
5: **else**Go to 3
6: **end if**

We present here, for two kind of exact solutions, the meshes obtained for the different estimators, with the same number of iterations.

2.5.1. *Example with peak function.* On the computational domain $[0,1]^2$, we consider a model problem with homogeneous data. With the source term f given by the exact solution,

$$u = xy(x-1)(y-1)e^{-100(x-0.5)^2-100(y-0.117)^2}$$

which presents sharp curvature in the vicinity of point $(0.5, 0.117)$, and we perform a non-conforming finite element discretization on it. We compare the results of adaptive refinement, also compare the effectivity index of η_1, η_2 and η_3. Successive iterations of adaptive mesh for the three estimators are represented in Figures 2, 3 and 4. The refinement occurs in the point $(0.5, 0.117)$ as expected. It shows that the three estimators captures the local distribution of the error similarly. The asymptotic decays of the three estimators are contrasted against the number of degrees of freedom (ndof) in Figure 5.We observe that the three estimators for this

example exhibit analogous behavior. Figure 6 compares the effectivity indices of all estimators. We observe that the effectivity indices takes roughly constant values for the three estimators.

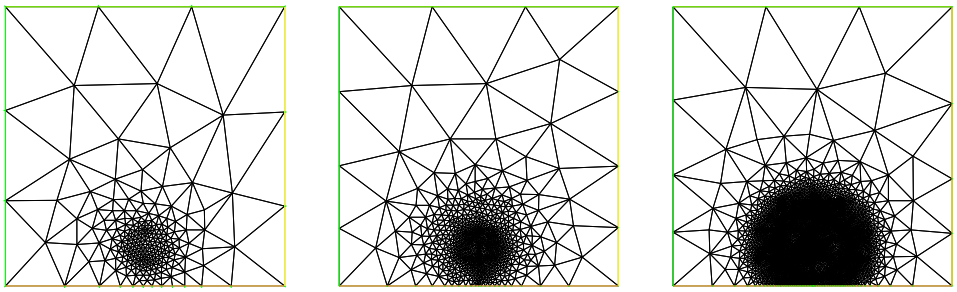

457 triangles
240 vertices

1684 triangles
859 vertices

12278 triangles
6176 vertices

FIGURE 2. Example 2.5.1. Adaptive mesh refinement using the error indicator for equilibration estimator.

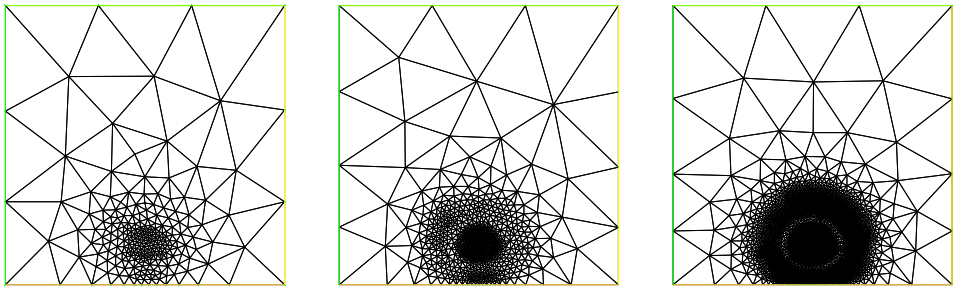

470 triangles
247 vertices

1607 triangles
821 vertices

11261 triangles
5662 vertices

FIGURE 3. Example 2.5.1. Adaptive mesh refinement using the error indicator for star-based estimator.

2.5.2. *Example with boundary layers.* Let Ω be the unit square, $\Omega = [0,1]^2$. We take the right-hand side f such that the exact solution is

$$u(x,y) = xy(1 - e^{(x-1)/\gamma})(1 - e^{(y-1)/\gamma}).$$

with boundary layer parameter $\gamma = 0.05$. Figures 7, 8 and 9 present successive iterations of adaptive mesh for the three estimators, the refinement occurs at both boundary layers located near the lines $x = 1$ and $y = 1$ as expected. We note that the star-based estimator capture the local distribution of the error better than the two other estimators. The asymptotic decays of the three estimators versus the ndof are compared in figure 10. For this example, the three estimators show analogous behavior. . Figure 11 compares the effectivity indices of all estimators. We observe that the effectivity indices takes roughly constant values for the three estimators.

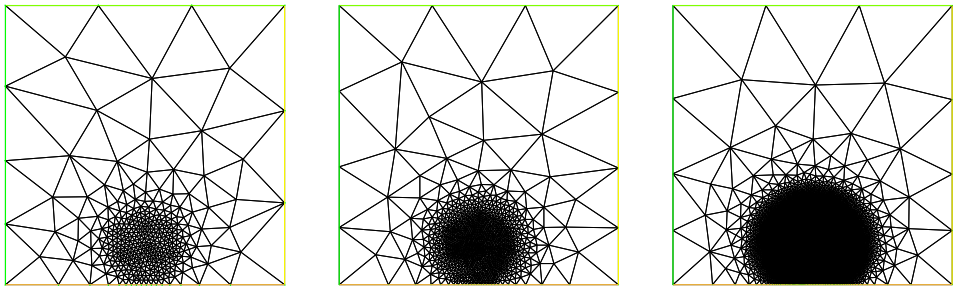

707 triangles
368 vertices

2271 triangles
1156 vertices

15527 triangles
7804 vertices

FIGURE 4. Example 2.5.1. Adaptive mesh refinement using the error indicator for residual estimator.

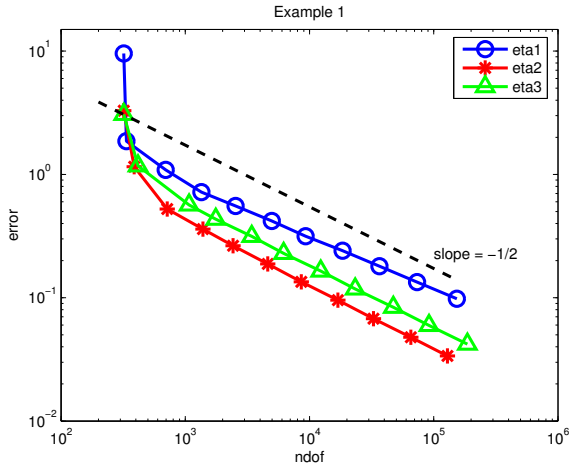

FIGURE 5. Example 2.5.1. Experimental convergence rates for the three a posteriori error estimators plotted against the number of degrees of freedom.

Figures 5 and 10 indicate quasi-optimality of the estimators, the dashed line of slope $(-1/2)$ showing a numerical $(ndof)^{-1/2}$ asymptotic decay of the three estimators.

3. Stokes problem

3.1. Problem setting, notations and discrete problem. Let Ω be an open bounded of $\mathbb{R}^d$, $d = 2, 3$, with a polygonal (Polyhedral) Lipschitz boundary Γ. We consider the Stokes problem : given $\boldsymbol{f} \in [L^2(\Omega)]^d$, find $\boldsymbol{u}$, the "velocity", and p, the "pressure", such that

$$\begin{cases} -\Delta \boldsymbol{u} + \nabla p = \boldsymbol{f} & in\ \Omega, \\ \nabla \cdot \boldsymbol{u} = 0 & in\ \Omega, \\ \boldsymbol{u} = \boldsymbol{0} & on\ \Gamma. \end{cases} \tag{3.1}$$

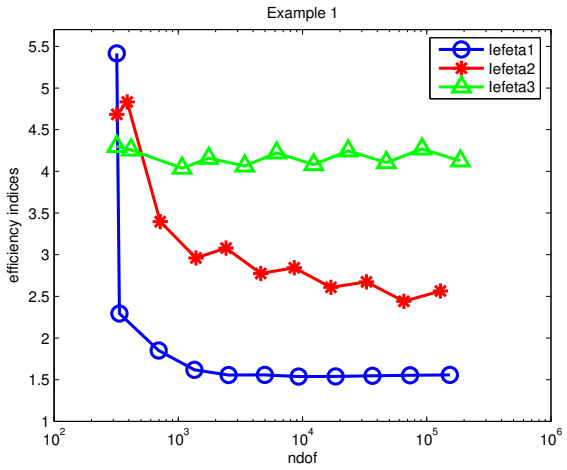

FIGURE 6. Example 2.5.1. Effectivity indices of the three a posteriori error estimators plotted against the number of degrees of freedom.

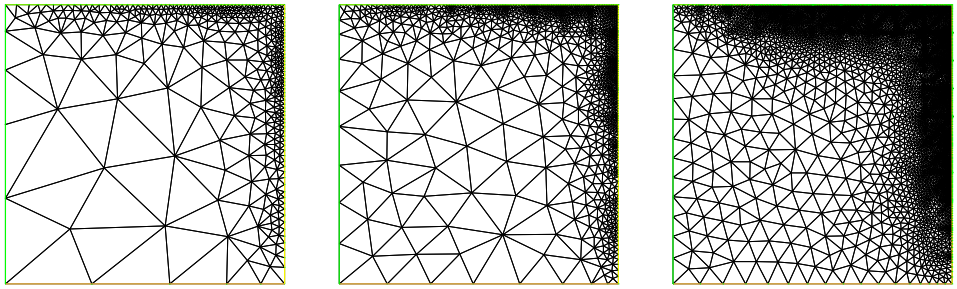

730 triangles
428 vertices

2366 triangles
1293 vertices

14590 triangles
7504 vertices

FIGURE 7. Example 2.5.2. Adaptive mesh refinement using the error indicator for equilibration estimator.

Throughout this section, we employ standard notation for the Lebesgue $L^2(\Omega)$ and Sobolev $(H_0^1(\Omega))^d$ spaces. The scalar product in $L^2(\Omega)$ is denoted by $(\cdot,\cdot)$ and its norm by $\|\cdot\|_{0,\Omega}$. Let $\boldsymbol{u} = [u_i]_{i=1,d}$, $\boldsymbol{v} = [v_i]_{i=1,d}$ be two vectors, and $\boldsymbol{A} = [A_{ij}]_{i,j=1,d}$, $\boldsymbol{B} = [B_{ij}]_{i,j=1,d}$ be two matrices, define

$$\nabla \boldsymbol{u} := [\partial_j u_i]_{i,j=1,d}, \qquad \nabla \cdot \boldsymbol{u} := \sum_{i=1}^{d} \partial_i u_i,$$

$$\boldsymbol{u} \otimes \boldsymbol{v} := [u_i v_j]_{i,j=1,d}, \qquad \operatorname{div} \boldsymbol{A} := [\sum_{j=1}^{d} \partial_j A_{ij}]_{i=1,d},$$

$$\boldsymbol{A} : \boldsymbol{B} = \sum_{i,j=1}^{d} A_{ij} B_{ij}.$$

To establish the weak form of the above system, we introduce the following spaces :

$$\boldsymbol{V} = (H_0^1(\Omega))^d, M = \{q \in L^2(\Omega) \mid \int_\Omega q \, dx = 0\}.$$

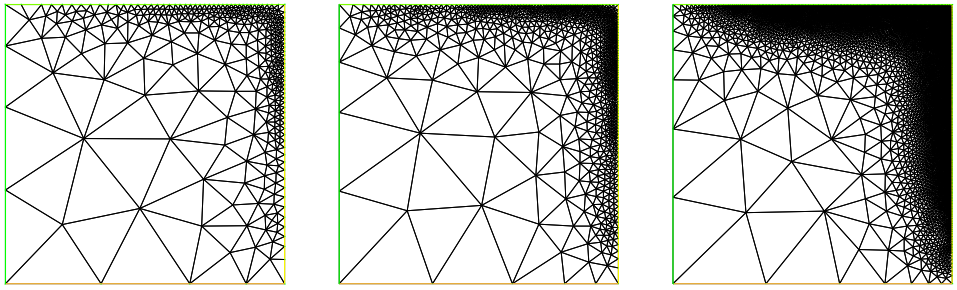

682 triangles
389 vertices

2077 triangles
1119 vertices

12949 triangles
6651 vertices

FIGURE 8. Example 2.5.2. Adaptive mesh refinement using the error indicator for star-based estimator.

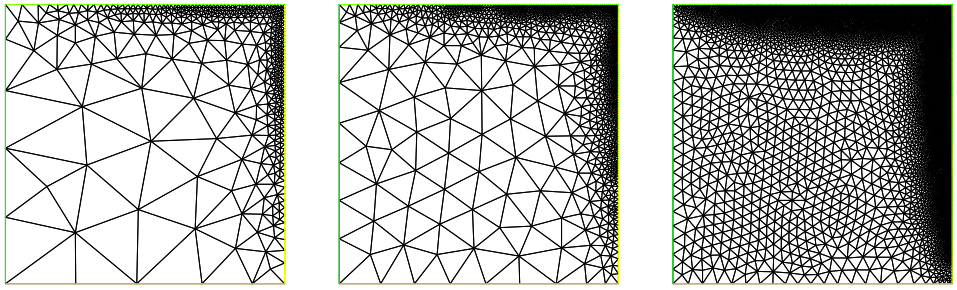

809 triangles
467 vertices

2199 triangles
1208 vertices

13807 triangles
7145 vertices

FIGURE 9. Example 2.5.2. Adaptive mesh refinement using the error indicator for residual estimator.

Then the standard variational formulation of problem (3.1) is given by the following :

$$\begin{cases} \text{find } \boldsymbol{u} \in \boldsymbol{V} \text{ and } p \in M \text{ such that} \\ \\ B((\boldsymbol{u},p);(\boldsymbol{v},q)) = (\boldsymbol{f},\boldsymbol{v}) \quad \forall (\boldsymbol{v},q) \in \boldsymbol{V} \times M, \end{cases} \tag{3.2}$$

where

$$B((\boldsymbol{u},p);(\boldsymbol{v},q)) = a(\boldsymbol{u},\boldsymbol{v}) + b(\boldsymbol{v},p) + b(\boldsymbol{u},q),$$

with the continuous bilinear forms

$$a(\boldsymbol{u},\boldsymbol{v}) = \int_\Omega \nabla \boldsymbol{u} : \nabla \boldsymbol{v}\, dx, \qquad b(\boldsymbol{v},p) = -\int_\Omega p\, \nabla \cdot \boldsymbol{v}\, dx$$

It is well-known that the weak formulation of the Stokes problem is well-posed [36]. We define the spaces

$$\mathbf{V}_h^d = (V_h)^d, \quad Q_h = \{q_h \in L_0^2(\Omega), q_{h|T} \in P_0(T), \forall T \in \mathcal{T}_h\}. \tag{3.3}$$

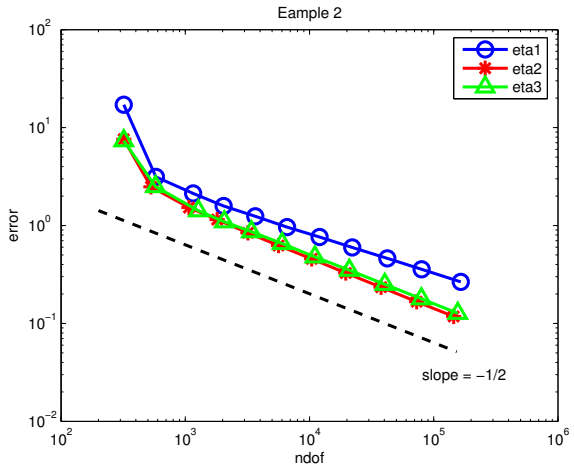

FIGURE 10. Example 2.5.2. Experimental convergence rates for the three a posteriori error estimators plotted against the number of degrees of freedom.

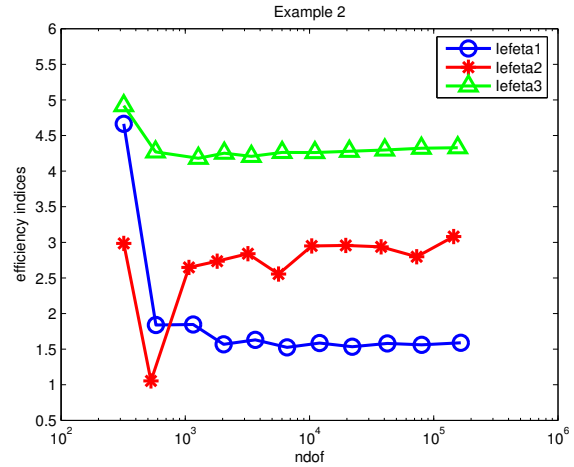

FIGURE 11. Example 2.5.2. Effectivity indices of the three a posteriori error estimators plotted against the number of degrees of freedom.

The nonconforming finite element approximation of the problem (3.1) is as follows :

$$\begin{cases} \text{find } \boldsymbol{u}_h^{NC} \in \mathbf{V}_h^d \text{ and } p_h \in Q_h \text{ such that} \\ \forall \boldsymbol{v}_h \in (V_h)^d, \quad \sum_{T \in \mathcal{T}_h} \left\{ \int_T \nabla \boldsymbol{u}_h^{NC} : \nabla \boldsymbol{v}_h \, dx - \int_T p_h \operatorname{div} \boldsymbol{v}_h \, dx \right\} = \int_\Omega \boldsymbol{f} \cdot \boldsymbol{v}_h \, dx, \\ \forall q_h \in Q_h, \quad \sum_{T \in \mathcal{T}_h} \int_T q_h \operatorname{div} \boldsymbol{u}_h^{NC} \, dx = 0. \end{cases} \tag{3.4}$$

3.2. Equilibration estimator. In this subsection we present an a posteriori error estimator developed by Achchab et al. in [1] for the nonconforming approximation of the Stokes problem. This estimator is based on the flux reconstruction approach described in (2.2), here the authors extended this method to the Stokes problem.

For all $T \in \mathcal{T}_h$, we consider the field $\boldsymbol{\sigma}_h$, defined locally as follows

$$\boldsymbol{\sigma}_h = \nabla \boldsymbol{u}_h^{NC} - \frac{1}{d} \boldsymbol{f}_h \otimes (\boldsymbol{x} - \boldsymbol{x}_G), \tag{3.5}$$

where $\boldsymbol{f}_h|_T := \boldsymbol{f}_T = \dfrac{1}{meas_d(T)} \displaystyle\int_T \boldsymbol{f}\, dx,\ \forall T \in \mathcal{T}_h$ and $\boldsymbol{x}_G$ is the barycenter of T. We introduce the local indicator and the global estimator defined respectively by

$$\eta_T^2 = \|\nabla \tilde{\boldsymbol{u}}_h - \boldsymbol{\sigma}_h\|_{0,T}^2 + \|\mathbf{div}\ \tilde{\boldsymbol{u}}_h\|_{0,T}^2 \quad and \quad \mathcal{E}_h^2 = \sum_{T \in \mathcal{T}_h} \eta_T^2. \tag{3.6}$$

The data oscillation is defined by

$$osc_1(\boldsymbol{f}) = \Big(\sum_{T \in \mathcal{T}_h} h_T^2 \|\boldsymbol{f}_h - \boldsymbol{f}\|_{0,T}^2 \Big)^{1/2}. \tag{3.7}$$

We recall the following result from [1].

Theorem 3.1. *Let $(\tilde{\boldsymbol{u}}_h, p_h) \in (H_0^1(\Omega)^d \cap V_h^d) \times M_h$, where $\tilde{\boldsymbol{u}}_h$ is a conforming post-processing of $\boldsymbol{u}_h^{NC}$ obtained by using the Oswald interpolation operator. we suppose that*

$$\|p - p_h\|_{0,\Omega} \leq C |\boldsymbol{u} - \tilde{\boldsymbol{u}}_h|_{1,\Omega},$$

where C is a positive constant depends on the triangulation $\mathcal{T}_h$ and the domain Ω. Then the next estimate holds

$$|\boldsymbol{u} - \tilde{\boldsymbol{u}}_h|_{1,\Omega}^2 + \|\nabla \boldsymbol{u} - \boldsymbol{\sigma}_h\|_{0,\Omega}^2 \leq C_5 \left\{ \mathcal{E}_h^2 + osc_1(\boldsymbol{f})^2 \right\} \tag{3.8}$$

and

$$\eta_T \leq C_6 \{ |\boldsymbol{u} - \tilde{\boldsymbol{u}}_h|_{1,T} + \|\nabla \boldsymbol{u} - \boldsymbol{\sigma}_h\|_{0,T} \},\ \ \forall T \in \mathcal{T}_h, \tag{3.9}$$

where C_5 and C_6 are a positive constants independent of h.

3.3. Star-based estimator. In this subsection we present an extension of the ideas given in subsection (2.3) to the Stokes equations by adapting introduced arguments.
We introduce the following local problems :

$$(SP_i) \begin{cases} \text{Find } \epsilon_i \in (\mathcal{P}_0^2(\omega_i))^2 \text{ such that} \\ \forall \mu_i \in (\mathcal{P}_0^2(\omega_i))^2,\ \displaystyle\int_{\omega_i} (\nabla \epsilon_i : \nabla \mu_i) \phi_i\, dx = \int_{\omega_i} \nabla_h \boldsymbol{u}_h^{NC} : \nabla(\mu_i \phi_i)\, dx \\ \qquad - \displaystyle\int_{\omega_i} p_h \operatorname{div}(\mu_i \phi_i)\, dx - \int_{\omega_i} (\boldsymbol{f} \cdot \mu_i) \phi_i\, dx. \end{cases}$$

It is evident that these local problems admit unique solutions.
We introduce the three indicators for all $i \in \mathcal{N}$,

$$\eta_{1,i}(\boldsymbol{u}_h^{NC}, p_h) = \Big(\sum_{T\in\omega_i} \| \operatorname{div} \boldsymbol{u}_h^{NC}\phi_i^{\frac{1}{2}}\|_{0,T}^2\Big)^{\frac{1}{2}}, \tag{3.10}$$

$$\eta_{2,i}(\boldsymbol{u}_h^{NC}, p_h) = \Big(\int_{\omega_i} |\nabla e_i|^2\phi_i\, dx\Big)^{\frac{1}{2}}, \tag{3.11}$$

$$\eta_{3,i}^2(\boldsymbol{u}_h^{NC}, p_h) = \sum_{E\in\omega_i} h^{-1}||[\boldsymbol{u}_h^{NC}]_E||_{0,E}, \tag{3.12}$$

and set the problem data oscillation,

$$osc_2(\boldsymbol{f}) = \Big(\sum_{i\in\mathcal{N}} h_i^2\|(\boldsymbol{f}-\boldsymbol{f}_i)\phi_i^{\frac{1}{2}}\|_{0,\omega_i}^2\Big)^{\frac{1}{2}}, \tag{3.13}$$

where $\boldsymbol{f}_i = \dfrac{\int_{\omega_i}\boldsymbol{f}\phi_i\, dx}{\int_{\omega_i}\phi_i\, dx}$ for interior nodes, and $\boldsymbol{f}_i = \mathbf{0}$ otherwise.

The following theorem [4] provides the a posteriori error estimate for the nonconforming finite element approximation of Stokes problem solution.

Theorem 3.2. *There exists a positive constant C_7 depending on the minimum angle of the triangulation such that :*

$$\Big(\sum_{i\in\mathcal{N}}\|\boldsymbol{u}-\boldsymbol{u}_h^{NC}\|_{1,\omega_i}^2\Big)^{\frac{1}{2}} + \|p-p_h\|_{0,\Omega} \le C_7\left\{\Big[\sum_{i\in\mathcal{N}}(\eta_{1,i}^2+\eta_{2,i}^2+\eta_{3,i}^2)\Big]^{\frac{1}{2}} + osc_2(\boldsymbol{f})\right\}, \tag{3.14}$$

For the estimator efficiency, we give the following theorem [4].

Theorem 3.3. *$\forall\omega_i \in \mathcal{T}_h$, there exist positive constants C_8, C_9 and C_{10} depending on the minimum angle of the triangulation such that :*

$$\| \operatorname{div}_h \boldsymbol{u}_h^{NC}\|_{0,\omega_i} \le C_8\|\boldsymbol{u}-\boldsymbol{u}_h^{NC}\|_{1,\omega_i}, \tag{3.15}$$

$$\eta_{2,i} \le C_9\Big(\|\boldsymbol{u}-\boldsymbol{u}_h^{NC}\|_{1,\omega_i} + \|p-p_h\|_{0,\omega_i}\Big), \tag{3.16}$$

and

$$\eta_{3,i} \le C_{10}\|u-u_h^{NC}\|_{1,\omega_i}. \tag{3.17}$$

3.4. Residual estimator. In this subsection we present residual-based error estimator developed by Dari et al. in [30] for the nonconforming approximation of the Stokes problem. We consider the same discrete problem as (3.4).

For a side E define $J_{E,n}$ and $J_{E,t}$ by

$$J_{E,n} = \begin{cases} [(\nabla\boldsymbol{u}_h^{NC} - p_h I)n]_E & \text{if} \quad E\in E_h^I \\ \\ 0 & \text{if} \quad E\in E_h^F \end{cases} \tag{3.18}$$

and

$$J_{E,t} = \begin{cases} [\nabla\boldsymbol{u}_h^{NC}t]_E & \text{if} \quad E\in E_h^I \\ \\ 2\nabla\boldsymbol{u}_h^{NC}t & \text{if} \quad E\in E_h^F \end{cases} \tag{3.19}$$

With this notation we introduce the local error estimator η_T defined by.

$$\eta_T^2(\boldsymbol{u}_h^{NC}, p_h) = meas_d(T)\|\boldsymbol{f}\|_{0,T}^2 + \frac{1}{2}\sum_{E\in E_T} h_E^2(|J_{E,n}|^2 + |J_{E,t}|^2), \tag{3.20}$$

Finally, the global error estimator is given by

$$\eta^2 = \sum_{T\in\mathcal{T}_h} \eta_T^2.$$

The data oscillation is defined by

$$osc_3(\boldsymbol{f}) = \Big(\sum_{T\in\mathcal{T}_h} meas_d(T)\|(\boldsymbol{f} - \boldsymbol{f}_h)\|_{0,T}^2\Big)^{\frac{1}{2}}, \tag{3.21}$$

For a piecewise regular vector function $\boldsymbol{v}_h$ we define the discrete gradient as the L^2-matrix defined by

$$\nabla_h \boldsymbol{v}_h|T = \nabla(\boldsymbol{v}_h|T).$$

The following theorem [30] provides The upper bound of the error.

Theorem 3.4. *Let $(\boldsymbol{u}, p)$ be the solution of the Stokes problem (3.2), and let $(\boldsymbol{u}_h^{NC}, p_h) \in V_h^d \times Q_h$ be a solution of the discrete problem (3.4). There exists a positive constant C_{11} such that*

$$\|\nabla_h(\boldsymbol{u} - \boldsymbol{u}_h^{NC})\|_{0,\Omega} + \|p - p_h\|_{0,\Omega} \leq C_{11}\eta. \tag{3.22}$$

Next, we show a local lower bound on the estimator [30] :

Theorem 3.5. *Let $(\boldsymbol{u}, p)$ be the solution of the Stokes problem (3.2), and let $(\boldsymbol{u}_h^{NC}, p_h) \in V_h^d \times Q_h$ be a solution of the discrete problem (3.4). There exists a positive constant C_{12} such that*

$$\eta \leq C_{12}(\|\nabla_h(\boldsymbol{u} - \boldsymbol{u}_h^{NC})\|_{0,\Omega} + \|p - p_h\|_{0,\Omega} + osc_3(\boldsymbol{f})). \tag{3.23}$$

3.5. Numerical experiments. In this subsection, we compare all the estimators we have presented for the Stokes problem and that we will denote as follows

$$\eta_1 := \Big\{\mathcal{E}_h^2 + osc_1(\boldsymbol{f})^2\Big\}^{\frac{1}{2}} \tag{3.24}$$

$$\eta_2 := \Big[\sum_{i\in\mathcal{N}}(\eta_{1,i}^2 + \eta_2^2) + \eta_3^2\Big]^{\frac{1}{2}} + osc_2(\boldsymbol{f}), \tag{3.25}$$

$$\eta_3 := \left(\sum_{T\in\mathcal{T}_h}(meas_d(T)\|\boldsymbol{f}\|_{0,T}^2 + \frac{1}{2}\sum_{E\in E_T} h_E^2(|J_{E,n}|^2 + |J_{E,t}|^2)\right)^{\frac{1}{2}}. \tag{3.26}$$

They are tested with using the Algortithm 1. We present here, for two kind of exact solutions, the meshes obtained for the different estimators, with the same number of iterations.

3.5.1. *L-shape domain problem.* The first example is a flow problem in the L-shape domain $\Omega = [-1,1]^2 - [0,1]^2$. The right hand side $\boldsymbol{f}$ of the Stokes problem (3.1) is determined by exact velocity $\boldsymbol{u} = (u_1, u_2)$ and pressure p :

$$u_1(x,y) = \frac{y-0.1}{\sqrt{(x-0.1)^2+(y-0.1)^2}},$$
$$u_2(x,y) = \frac{x-0.1}{\sqrt{(x-0.1)^2+(y-0.1)^2}},$$
$$p(x,y) = \frac{1}{y+1.05} - \frac{\log(2.05)+\log(1.05)-2\log(0.05)}{3}.$$

We note that both the velocity $\boldsymbol{u}$ and the pressure p are smooth in the domain. However, it is clear that $\boldsymbol{u}$ and p are singular at the point $(0.1, 0.1)$ and along the line $y = -1.05$, respectively. Figures 12, 13 and 14 present successive iterations of adaptive mesh for the three estimators, we can see the refined meshes appear around the origin and along the line $y = -1$, which are near the locations of singularity. It shows that the three estimators captures the local distribution of the error similarly. Figures 15 to 20 present adaptive computed velocity and adaptive computed pressure respectively for the three error indicators. Figure 21 gives comparison of asymptotic decays of the three estimators versus the ndof. We note analogous behavior of the three estimators for this example. Figure 22 compares the effectivity indices of all estimators where their asymptotic values are found to be fairly constant.

3.5.2. *A singular problem.* The second example is taken from [39]. The domain is the rectangle $\Omega = [-1,1] \times [0,1]$. The exact solution is given by

$$u_e = \frac{3\sqrt{r}}{2}\left(cos\frac{\theta}{2} - cos\frac{3\theta}{2}, 3sin\frac{\theta}{2} - sin\frac{3\theta}{2}\right),$$
$$p_e = -\frac{6}{\sqrt{r}}cos\frac{\theta}{2},$$

where (r,θ) are the polar coordinates in Ω. The solution has a singularity at the origin $(0,0)$. Figures 23, 24 and 25 present successive iterations of adaptive mesh using η_1, η_2 and η_3 as local refinement indicators. It can be seen that all three estimators capture the singularity at the origin as expected. Figures 26 to 31 present adaptive computed velocity and adaptive computed pressure respectively for the three error indicators. Figure 32 gives comparison of asymptotic decays of the three estimators versus the ndof. We note analogous behavior of the three estimators for this example. Figure 33 compares the effectivity indices of all estimators, We observe that the effectivity indices takes roughly constant values.
Figures 21 and 32 illustrates quasi-optimality of the three estimators, the dashed line of slope $(-\frac{1}{2})$ showing a numerical $(ndof)^{-\frac{1}{2}}$ asymptotic decay of the three estimators.

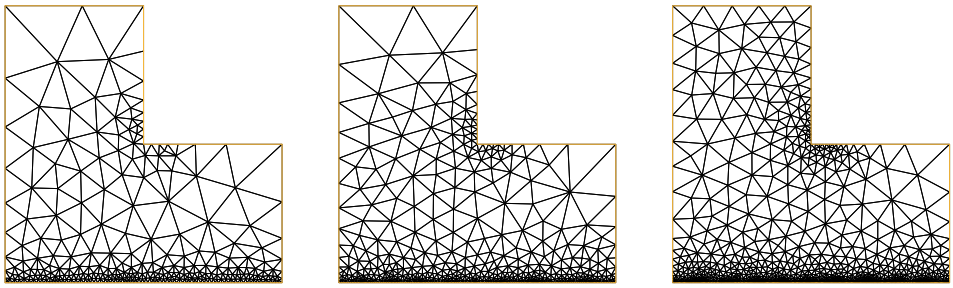

570 triangles
344 vertices

1027 triangles
625 vertices

2119 triangles
1236 vertices

FIGURE 12. Example 3.5.1. Adaptive mesh refinement using the error indicator for equilibration estimator.

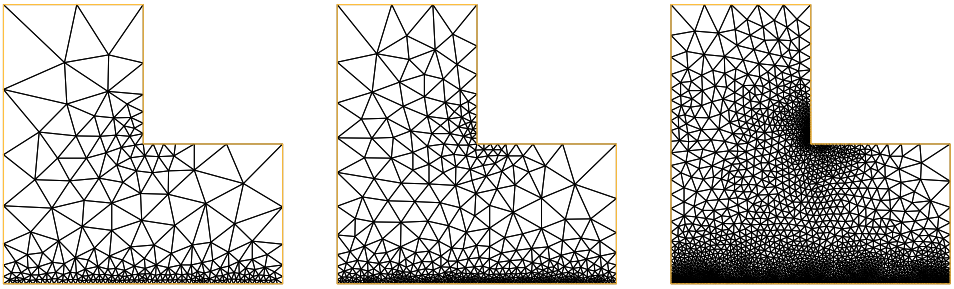

488 triangles
293 vertices

1131 triangles
638 vertices

4807 triangles
2546 vertices

FIGURE 13. Example 3.5.1. Adaptive mesh refinement using the error indicator for star-based estimator.

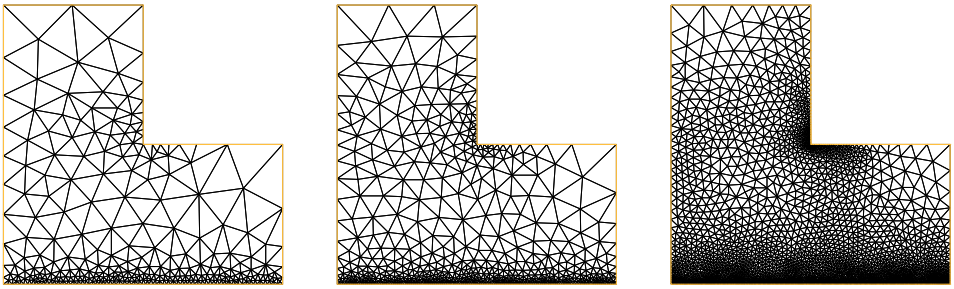

568 triangles
340 vertices

1266 triangles
727 vertices

5795 triangles
3088 vertices

FIGURE 14. Example 3.5.1. Adaptive mesh refinement using the error indicator for residual estimator.

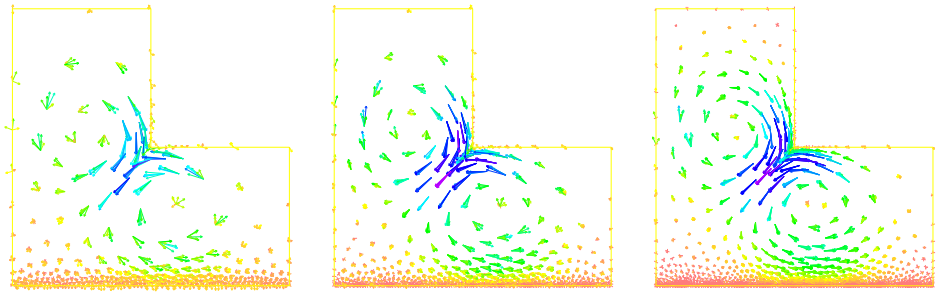

FIGURE 15. Example 3.5.1. Adaptive computed velocity using the error indicator for equilibration estimator.

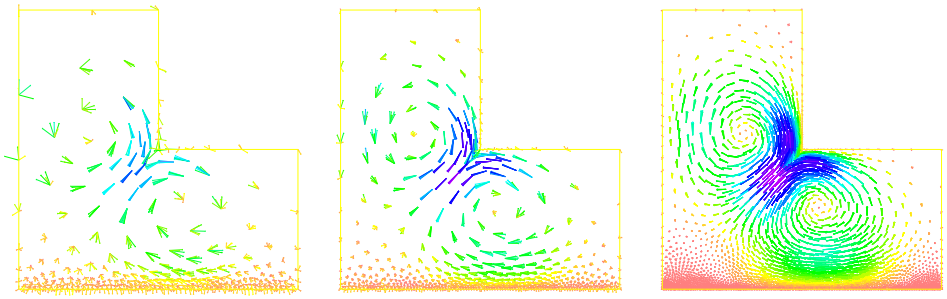

FIGURE 16. Example 3.5.1. Adaptive computed velocity using the error indicator for star-based estimator.

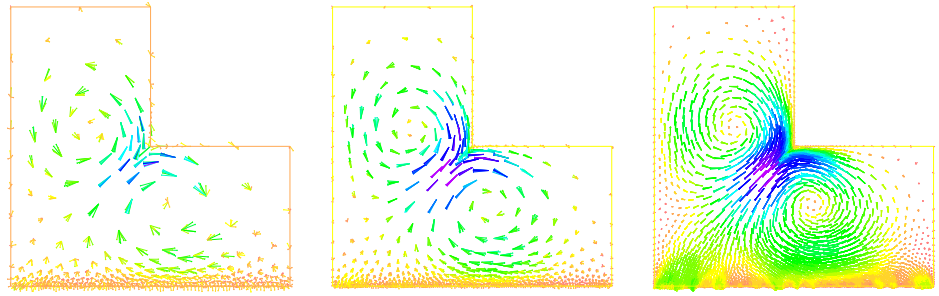

FIGURE 17. Example 3.5.1. Adaptive computed velocity using the error indicator for residual estimator.

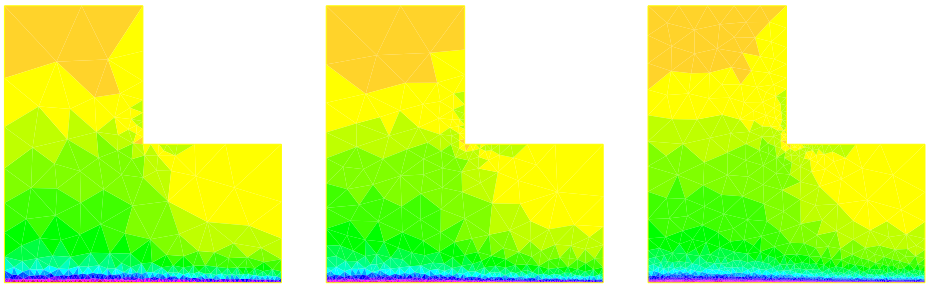

FIGURE 18. Example 3.5.1. Adaptive computed pressure using the error indicator for equilibration estimator.

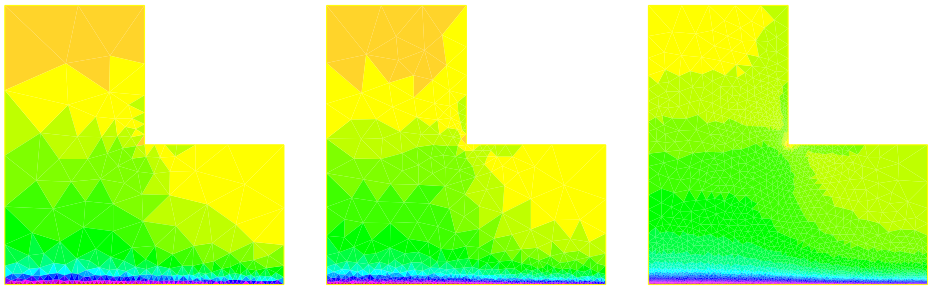

FIGURE 19. Example 3.5.1. Adaptive computed pressure using the error indicator for star-based estimator.

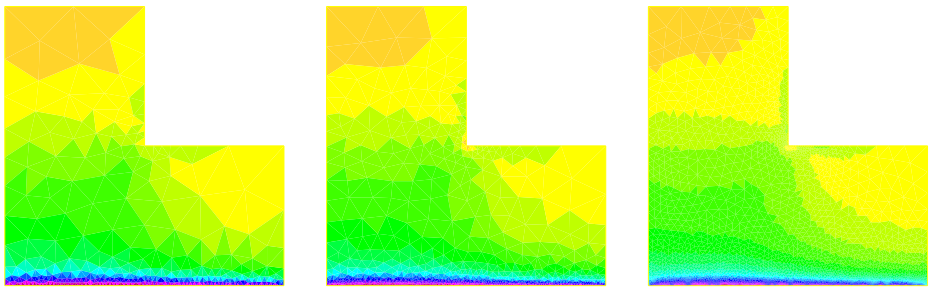

FIGURE 20. Example 3.5.1. Adaptive computed pressure using the error indicator for residual estimator.

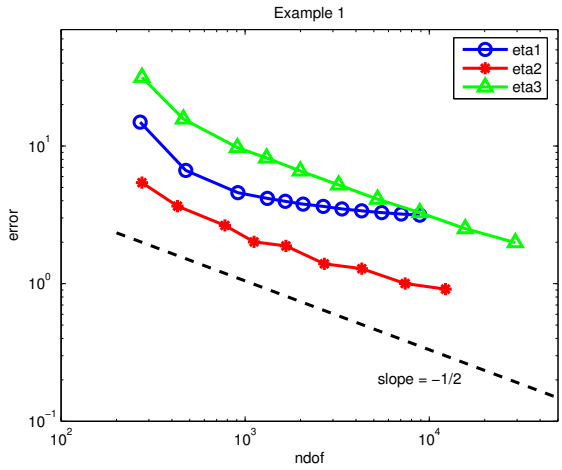

FIGURE 21. Example 3.5.1. Experimental convergence rates for the three a posteriori error estimators plotted against the number of degrees of freedom.

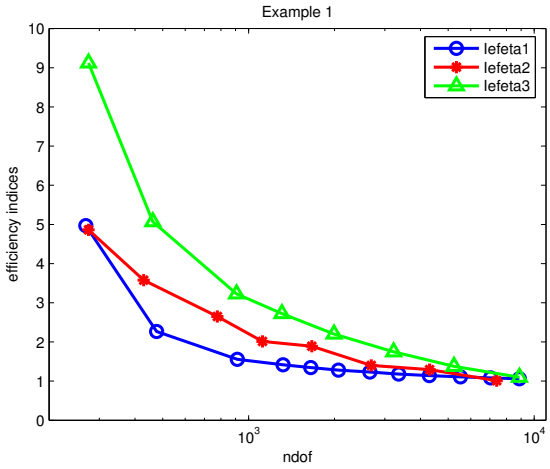

FIGURE 22. Example 3.5.1. Efficiency indices of the three a posteriori error estimators plotted against the number of degrees of freedom.

4. Conclusion

We compared three types of a posteriori error estimators for the Poisson problem and the Stokes problem. It may be noted that the behavior of these estimators differs between the two problems. For the Poisson problem, the estimator based on the resolution of local problems

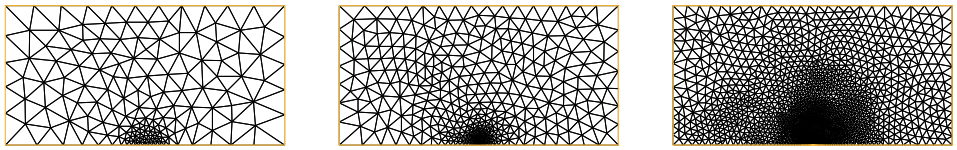

305 triangles
176 vertices

842 triangles
460 vertices

4311 triangles
2242 vertices

FIGURE 23. Example 3.5.2. Adaptive mesh refinement using the error indicator for equilibration estimator.

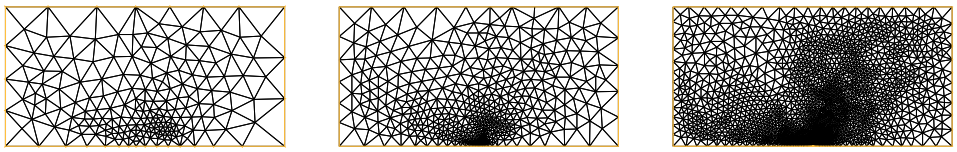

375 triangles
203 vertices

1054 triangles
553 vertices

5283 triangles
2702 vertices

FIGURE 24. Example 3.5.2. Adaptive mesh refinement using the error indicator for star-based estimator.

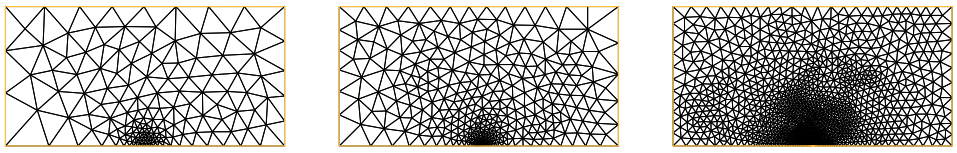

281 triangles
161 vertices

711 triangles
389 vertices

3256 triangles
1699 vertices

FIGURE 25. Example 3.5.2. Adaptive mesh refinement using the error indicator for residual estimator.

better detects the singularity than the other two estimators, even if it takes more time in the calculation. On the other hand, the effectivity index of the estimator based on the equilibrated flux is closer to 1 than the other two. For the Stokes problem, the estimator based on the equilibrated flux better localizes the singularity than the other two estimators, we also note that the estimator based on the resolution of local problems converges faster than the other two.

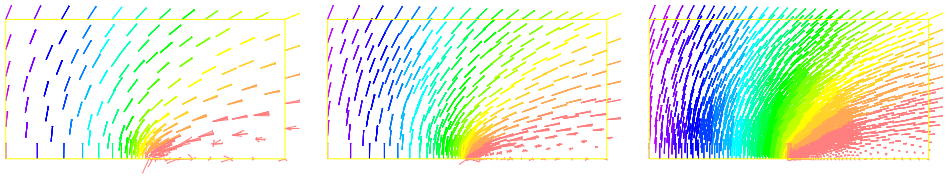

FIGURE 26. Example 3.5.2. Adaptive computed velocity using the error indicator for equilibration estimator.

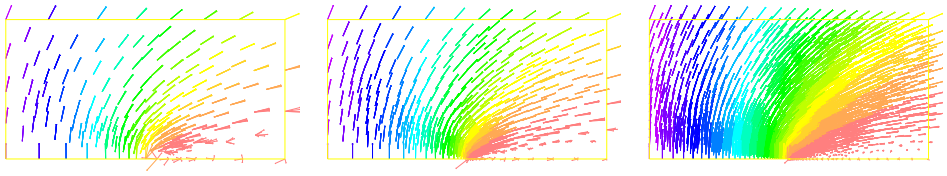

FIGURE 27. Example 3.5.2. Adaptive computed velocity using the error indicator for star-based estimator.

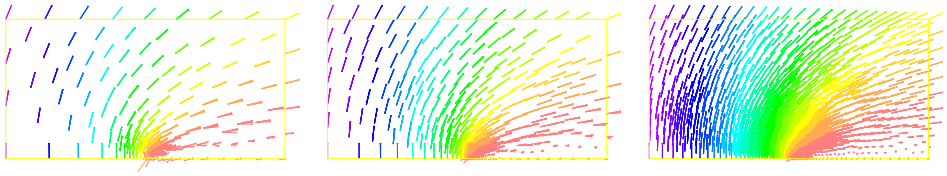

FIGURE 28. Example 3.5.2. Adaptive computed velocity using the error indicator for residual estimator.

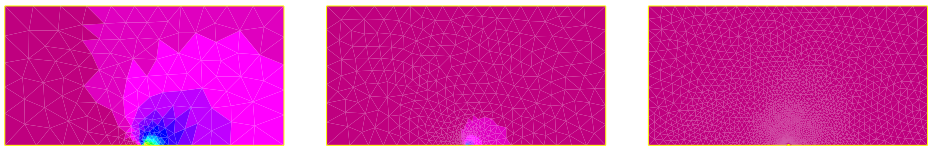

FIGURE 29. Example 3.5.2. Adaptive computed pressure using the error indicator for equilibration estimator.

References

[1] B. Achchab, A. Agouzal, J. Baranger, and F. Oudin. Estimations d'erreurs en lois de comportement. *Comptes Rendus de l'Académie des Sciences-Séries I-Mathematics*, 326(8):1007–1010, 1998.

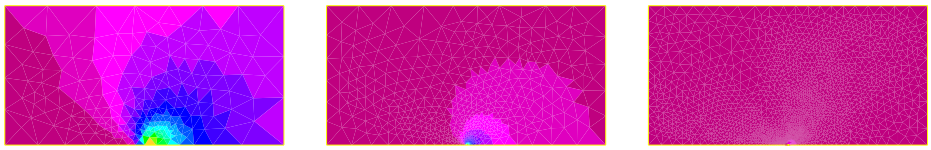

FIGURE 30. Example 3.5.2. Adaptive computed pressure using the error indicator for star-based estimator.

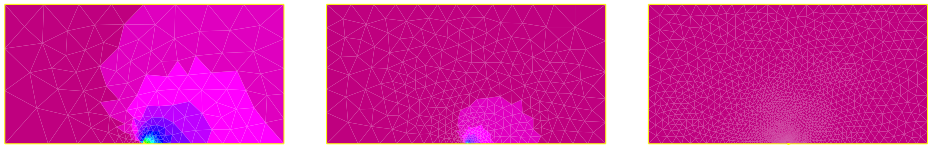

FIGURE 31. Example 3.5.2. Adaptive computed pressure using the error indicator for residual estimator.

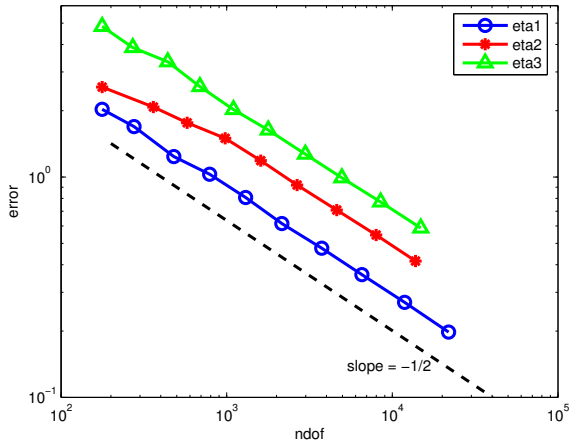

FIGURE 32. Example 3.5.2. Experimental convergence rates for the three a posteriori error estimators plotted against the number of degrees of freedom.

[2] B. Achchab, A. Agouzal, and K. Bouihat. A posteriori error estimates for non conforming approximation of quasi Stokes problem. *Revue Africaine de la Recherche en Informatique et Mathématiques Appliquées*, 16:47–66, 2013.

[3] B. Achchab, A. Agouzal, and K. Bouihat, A. Majdoubi and A. Souissi. Projection stabilized nonconforming finite element methods for the Stokes problem. *Numerical Methods for Partial Differential Equations* , 33(1):218–240, 2017.

[4] B. Achchab, A. Agouzal, N. Debit, and K. Bouihat. Star-based a posteriori error estimates for elliptic problems. *Journal of Scientific Computing*, 60(1):184–202, 2014.

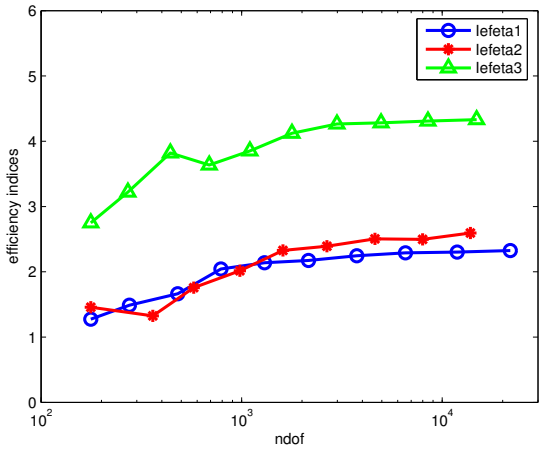

FIGURE 33. Example 3.5.2. Efficiency indices of the three a posteriori error estimators plotted against the number of degrees of freedom.

[5] B. Achchab, A. Agouzal, A. Majdoubi, D. Meskine, and A. Souissi. A posteriori error analysis for nonconforming approximations of an anisotropic elliptic problem. *Numerical Methods for Partial Differential Equations*, 31(3):950–976, 2015.

[6] B. Achchab, A. Majdoubi, D. Meskine, and A. Souissi. A posteriori error analysis using the constitutive law for the Crouzeix–Raviart element. *Applied Mathematics Letters*, 22(8):1309–1314, 2009.

[7] A. Agouzal. A posteriori error estimator for nonconforming finite element methods. *Applied Mathematics Letters*, 7(5):61 – 66, 1994.

[8] A. Agouzal. A posteriori error estimators for nonconforming approximation. *Mathematical Modelling and Numerical Analysis*, 5(1):77–85, 2008.

[9] M. Ainsworth. Robust a posteriori error estimation for nonconforming finite element approximation. *SIAM Journal on Numerical Analysis*, 42(6):2320–2341, 2005.

[10] D. Alsheikh and T. Katsaounis. A posteriori error estimators for discontinuous Galerkin method for diffusion problems, based on the hypercircle method. *Arabian Journal of Mathematics*, 11(3):407–426, 2022.

[11] I Babuška and C. Rheinboldt. Error estimates for adaptive finite element computations. *SIAM Journal on Numerical Analysis*, 15(4):736–754, 1978.

[12] R.E. Bank and A. Weiser. Some a posteriori error estimators for elliptic partial differential equations. *Mathematics of Computation*, 44(170):283–301, 1985.

[13] R. E Bank and B.D. Welfert. A posteriori error estimates for the Stokes equations: a comparison. *Computer Methods in Applied Mechanics and Engineering*, 82(1-3):323–340, 1990.

[14] R.E. Bank and B.D. Welfert. A posteriori error estimates for the Stokes problem. *SIAM Journal on Numerical Analysis*, 28(3):591–623, 1991.

[15] C. Bernardi, B. Métivet, and R; Verfürth. Analyse numérique d'indicateurs d'erreur. *in Maillage et adaptation. P.-L. George Ed., Hermès*, pages 251–278, 2001.

[16] K. Bouihat. Estimations d'erreurs pour les méthodes des éléments finis non conformes et des volumes finis [Error estimates for non conforming finite element and finite volume methods]. *Phd, University Hassan 1, Faculty of Science and Technology, Settat*, May 2012.

[17] D. Braess. An a posteriori error estimate and a comparison theorem for the nonconforming P_1 element. *Calcolo*, 46(2):149–155, 2009.

[18] D. Braess and J. Schöberl. Equilibrated residual error estimator for edge elements. *Mathematics of Computation*, 77(262):651–672, 2008.

[19] E. Burman and A. Ern. Continuous interior penalty hp-finite element methods for advection and advection-diffusion equations. *Mathematics of Computation*, 76(259):1119–1140, 2007.
[20] C. Carstensen, R. Klose, and A. Orlando. Reliable and efficient equilibrated a posteriori finite element error control in elastoplasticity and elastoviscoplasticity with hardening. *Computer Methods in Applied Eechanics and Engineering*, 195(19):2574–2598, 2006.
[21] C. Carstensen and C. Merdon. Estimator competition for Poisson problems. *Journal of Computational Mathematics*, 28(3):309–330, 2010.
[22] C. Carstensen and C. Merdon. Computational survey on a posteriori error estimators for nonconforming finite element methods for the Poisson problem. *Journal of Computational and Applied Mathematics*, 249:74–94, 2013.
[23] C. Carstensen and C. Merdon. A posteriori error estimator competition for conforming obstacle problems. *Numerical Methods for Partial Differential Equations*, 29(2):667–692, 2013.
[24] C. Carstensen and S.A. Funken. Constants in Clément-interpolation error and residual based a posteriori estimates in finite element methods. *East-West Journal of Numerical Mathematics*, 8(3):153–175, 2000.
[25] C. Carstensen, T. Gudi, and M. Jensen. A unifying theory of a posteriori error control for discontinuous Galerkin fem. *Numerische Mathematik*, 112(3):363–379, 2009.
[26] C. Carstensen and C. Merdon. Computational survey on a posteriori error estimators for the Crouzeix-Raviart nonconforming finite element method for the Stokes problem. *Computational Methods in Applied Mathematics*, 14(1):35–54, 2014.
[27] P.G. Ciarlet. The finite element method for elliptic problems. *North-Holland, Amsterdam*, 1978.
[28] M. Crouzeix and P.-A. Raviart. Conforming and nonconforming finite element methods for solving the stationary Stokes equations i. *ESAIM: Mathematical Modelling and Numerical Analysis - Modélisation Mathématique et Analyse Numérique*, 7(R3):33–75, 1973.
[29] E. Dari, R. Duran, C. Padra, and V. Vampa. A posteriori error estimators for nonconforming finite element methods. *ESAIM: Mathematical Modelling and Numerical Analysis*, 30(4):385–400, 1996.
[30] E. Dari, R. Durán, and C. Padra. Error estimators for nonconforming finite element approximations of the Stokes problem. *Mathematics of Computation*, 64(211):1017–1033, 1995.
[31] P. Destuynder and B. Métivet. Explicit error bounds for a nonconforming finite element method. *SIAM Journal on Numerical Analysis*, 35(5):2099–2115 (electronic), 1998.
[32] W. Dörfler and M. Ainsworth. Reliable a posteriori error control for nonconforming finite element approximation of Stokes flow. *Mathematics of Computation*, 74(252):1599–1619, 2005.
[33] A. Ern, A. F. Stephansen, and M. Vohralík. Guaranteed and robust discontinuous Galerkin a posteriori error estimates for convection–diffusion–reaction problems. *Journal of Computational and Applied Mathematics*, 234(1):114–130, 2010.
[34] A. Ern and M. Vohralík. Flux reconstruction and a posteriori error estimation for discontinuous Galerkin methods on general nonmatching grids. *Comptes Rendus Mathematique*, 347(7):441–444, 2009.
[35] A. Ern and M. Vohralík. Four closely related equilibrated flux reconstructions for nonconforming finite elements. *Comptes Rendus Mathematique*, 351(1):77–80, 2013.
[36] V. Girault and P.-A. Raviart. Finite Element Methods for Navier-Stokes Equations. *Springer-Verlag*, Berlin, 1986.
[37] A. Hannukainen, R. Stenberg, and M. Vohralík. A unified framework for a posteriori error estimation for the Stokes problem. *Numerische Mathematik*, 122(4):725–769, 2012.
[38] O. A Karakashian and F. Pascal. A posteriori error estimates for a discontinuous Galerkin approximation of second-order elliptic problems. *SIAM Journal on Numerical Analysis*, 41(6):2374–2399, 2003.
[39] D. Kay and D. Silvester. A posteriori error estimation for stabilized mixed approximations of the Stokes equations. *SIAM Journal on Scientific Computing*, 21(4):1321–1336, 1999.
[40] K. Kim. A posteriori error analysis for locally conservative mixed methods. *Mathematics of Computation*, 76(257):43–66, 2007.
[41] P. Ladevèze and D. Leguillon. Error estimate procedure in the finite element method and applications. *SIAM Journal on Numerical Analysis*, 20(3):485–509, 1983.

[42] P. Morin, R. Nochetto, and K. Siebert. Local problems on stars: a posteriori error estimators, convergence, and performance. *Mathematics of Computation*, 72(243):1067–1097, 2003.
[43] W. Prager and J. L. Synge. Approximations in elasticity based on the concept of function space. *Quarterly of Applied Mathematics*, 5(3):241–269, 1947.
[44] Y. Shen, W. Gong, and N. Yan. Convergence of adaptive nonconforming finite element method for Stokes optimal control problems. *Journal of Computational and Applied Mathematics*, 412:114336, 2022.
[45] L. Sun and Y. Yang. The a posteriori error estimates and adaptive computation of nonconforming mixed finite elements for the Stokes eigenvalue problem. *Applied Mathematics and Computation*, 421:126951, 2022.
[46] A. Veeser and R. Verfürth. Explicit upper bounds for dual norms of residuals. *SIAM Journal on Numerical Analysis*, 47(3):2387–2405, 2009.
[47] R. Verfürth. A posteriori error estimation and adaptive mesh-refinement techniques. *Journal of Computational and Applied Mathematics*, 50(1):67 – 83, 1994.
[48] R. Verfürth. *A review of a posteriori error estimation and adaptive mesh-refinement techniques*, volume 1. Wiley-Teubner Chichester, 1996.
[49] R. Verfürth. Error estimates for some quasi-interpolation operators. *ESAIM: Mathematical Modelling and Numerical Analysis*, 33(4):695–713, 1999.
[50] M. Vohralík. Guaranteed and fully robust a posteriori error estimates for conforming discretizations of diffusion problems with discontinuous coefficients. *Journal of Scientific Computing*, 46(3):397–438, 2011.
[51] B. Wohlmuth and R. Hoppe. A comparison of a posteriori error estimators for mixed finite element discretizations by Raviart-Thomas elements. *Mathematics of Computation of the American Mathematical Society*, 68(228):1347–1378, 1999.